



1 Long-term water clarity patterns of lakes across China using Landsat 2 series imagery from 1985 to 2020

3 Xidong Chen ¹, Liangyun Liu ^{2,*}, Xiao Zhang ^{2,3}, Junsheng Li ^{2,3}, Shenglei Wang ², Yuan Gao
4 ⁴, Jun Mi ^{2,3}

5 1. North China University of Water Resources and Electric Power, Zhengzhou 450046, China;

6 2. Key Laboratory of Digital Earth Science, Aerospace Information Research Institute, Chinese Academy
7 of Sciences, Beijing 100094, China;

8 3. University of Chinese Academy of Sciences, Beijing 100049, China;

9 4. Beijing Normal University, Beijing 100091, China

10 * Corresponding author: Liangyun Liu, E-mail address: liuly@radi.ac.cn.

11
12 **Abstract:** Monitoring the water clarity of lakes is essential for the sustainable development of
13 human society. However, existing water clarity assessments in China have mostly focused on
14 lakes with areas > 1 km², and the monitoring periods were mainly in the 21st century. In order
15 to improve the understanding of spatiotemporal variations in lake clarity across China, based
16 on the Google Earth Engine cloud platform, a 30 m long-term LAke Water Secchi Depth (SD)
17 dataset (LAWS30) of China (1985–2020) was first developed using Landsat series imagery and
18 a robust water-color-parameter-based SD model. The LAWS30 dataset exhibited a good
19 performance compared with concurrent in situ SD datasets, with an R^2 of 0.86 and a root-mean-
20 square error of 0.225 m. Then, based on our LAWS30 dataset, long-term spatiotemporal
21 variations in SD for lakes > 0.01 km² ($N = 40,973$) across China were evaluated. The results show
22 that the SD of lakes with areas ≤ 1 km² exhibited a significant downward trend in the period
23 1985–2020, but the decline rate began to slow down and stabilized after 2001. In addition, the
24 SD of lakes with an area > 1 km² showed a significant downward trend before 2001, and began
25 to increase significantly afterwards. Moreover, in terms of the spatial patterns, the proportion
26 of small lakes (area ≤ 1 km²) showing a decreasing SD trend was the largest in the Mongolian–
27 Xinjiang Plateau Region (MXR) (about 30.0%), and the smallest in the Eastern Plain Region (EPR)
28 (2.6%). In contrast, for lakes > 1 km², this proportion was the highest in MXR (about 23.0%), and
29 the lowest in the Northeast Mountain Plain Region (NER) (16.1%). The LAWS30 dataset and
30 the spatiotemporal patterns of lake water clarity in our research can provide effective guidance
31 for the protection and management of lake environment in China.

32 **Keywords:** water clarity; Secchi Depth (SD); Landsat; Google Earth Engine; long-term

33 1. Introduction

34 Lakes are invaluable resources for human societies, providing value in terms of water
35 supply, energy production, commerce, food production, and human health (Bastviken et al.,
36 2011; Palmer et al., 2015). However, like many other ecosystems, lakes are sensitive to multiple
37 co-occurring environmental pressures, notably climate change, nutrient enrichment, organic
38 and inorganic pollution, and human activities (Brönmark and Hansson, 2002). Nowadays, with
39 the rapid development of the economy and the growth of the population in China, the
40 intensification of human activities and pollution from industry and agricultural production



41 have caused severe damage to lakes (Ma et al., 2014; Wang and Yang, 2019; Zhou et al., 2019).
42 According to recent research and national survey reports (Barnes, 2014; Wang and Yang, 2019;
43 Ministry of Ecology and Environment of the People's Republic of China, 2020), approximately
44 70% of inland water in China is polluted, 28% of the assessed lakes are eutrophic, and about 140
45 million people depend on getting water from unsafe open sources. The deterioration of the lake
46 ecosystem has threatened public health and the safety of both humans and aquatic organisms
47 (Guo, 2007). Therefore, effective monitoring and evaluation of the environment of lakes across
48 China is necessary.

49 Water clarity is one of the most intuitive, popular, and important parameters for describing
50 the optical components of water bodies (Carlson, 1977; Liu et al., 2020), and is generally
51 measured in terms of Secchi Depth (SD) (Odermatt et al., 2012; Carlson, 1977). Since water clarity
52 is co-determined by the suspended matter, planktonic algae, and colored dissolved organic
53 matter in the water column, it is usually adopted as a practical comprehensive metric for water
54 quality assessment (Kloiber et al., 2002; Mccullough et al., 2012). Although a variety of physical,
55 biological, and chemical parameters have been proposed to analyze the condition of water,
56 water clarity has been utilized for a century as an effective and simple metric (Cuffney et al.,
57 2000; Lee et al., 2018). Recently, water clarity was also recognized as an important parameter in
58 support of the United Nations Sustainable Development Goal SDG 6.3.2 evaluation reports
59 (Shen et al., 2020). Therefore, water clarity is a significant indicator that can be used to monitor
60 and evaluate the comprehensive conditions of water.

61 Today, with the development of remote sensing technology, significant numbers of satellite
62 images are continuously being acquired. Taking into account the high-frequency revisits, large
63 area of coverage, and the historical archive of remote sensing data available, increasing attention
64 has been paid to the applications of remote sensing datasets in water clarity assessments (Li et
65 al., 2020a; Liu et al., 2019; Xue et al., 2019). The evaluation of water clarity from a variety of ocean
66 color satellite sensors has been performed (Li et al., 2020a; Feng et al., 2019; Wang et al., 2018;
67 Shi et al., 2018). For example, Shen et al. (2020) used Sentinel-3 data to evaluate the water clarity
68 of 86 lakes (> 30 km²) in eastern China; Liu et al. (2021) estimated the SD (water clarity) trends
69 of lakes with an area > 50 km² in the Tibetan Plateau using MODIS data between 2000 and 2019.
70 However, due to the coarse spatial resolution and the relatively short-term historical archives of
71 these ocean color sensors, their applications were limited to large lakes and reservoirs, and the
72 study periods were concentrated in the past two decades (Li et al., 2020a). The statistics on lakes
73 with an area ≤ 1 km² are scant, and understanding of the variations in SD before the 21st century
74 is limited (Downing et al., 2012; Biggs et al., 2017; Li et al., 2020b). In order to improve the water
75 environment monitoring capability, 30 m Landsat series data have recently been used for SD
76 evaluation (Page et al., 2019; Dona et al., 2014). Because of the fine spatial resolution (30 m), long
77 historical archives (> 35 years), and suitability for water clarity assessment, Landsat series data
78 are considered to be "ideal" for the long-term and fine spatial resolution monitoring of lake SD
79 (Olmanson et al., 2008; Olmanson et al., 2016; Li et al., 2020a; Zhang et al., 2021b). For example,
80 Li et al. (2020a) utilized the Landsat series of images to monitor the SD trends in the Xin'anjiang
81 Reservoir between 1986 and 2016; Yin et al. (2021) tracked the SD changes in Taihu from 1984 to
82 2018 based on Landsat 5 and 8 images. Recently, in order to conduct the first high-spatial-
83 resolution investigation of lake SD across China, significant amounts of Landsat 8 data from
84 2014–2017 were used in the work of Song et al. (2020). However, these studies were limited to



85 individual areas or periods. Due to the requirement for huge amounts of computation and large
86 storage capabilities, as well as the need for a robust uniform SD model, there are very few
87 examples of national-scale long-term SD estimations using Landsat imagery (Yin et al., 2021;
88 Kloiber et al., 2002; Page et al., 2019).

89 Fortunately, with the emergence of the Google Earth Engine (GEE) cloud computing
90 platform (Gorelick et al., 2017), its high-performance, intrinsically parallel computing services
91 can easily meet the requirements for very large computational resources (Zhang et al., 2020;
92 Liangyun Liu et al., 2021). Additionally, because the GEE platform integrates multipetabyte
93 analysis-ready Landsat surface reflectance data, and these data are intercalibrated between
94 different Landsat sensors, it presents an opportunity to conduct long-term land surface analyses
95 at the pixel level (Racotin et al., 2020; Zhang et al., 2021b). Accordingly, a robust SD model is the
96 only requirement for fine-resolution, long-term SD evaluation across China. Lately, some
97 studies have found that the SD is well correlated with water color parameters (e.g., hue angle
98 and the Forel–Ule Index (FUI)) (Wang et al., 2021; Chen et al., 2021; Van Der Woerd and Wernand,
99 2018). Since water color parameters can be retrieved at the global scale and over long time spans
100 (Wang et al., 2021; Wang et al., 2018), it is possible to retrieve long-term water clarity over large
101 areas based on these parameters (Wang et al., 2021; Wang et al., 2020). For example, Wang et al.
102 (2020) recently developed a robust SD model based on water color parameters, and the model
103 was successfully applied to MODIS data to develop a nationwide 500 m long-term SD dataset
104 between 2000 and 2017. Accordingly, a feasible solution for high-spatial-resolution and long-
105 term SD estimation across China could be provided by incorporating the GEE cloud platform
106 and the water-color-parameter-based SD model.

107 Therefore, in order to provide a comprehensive understanding of nationwide
108 spatiotemporal variations in lake water clarity, we first developed a long-term 30 m LAke Water
109 SD dataset of China from 1985 to 2020 (LAWSD30) using Landsat series data and a water-color-
110 parameter-based SD algorithm with the assistance of the GEE cloud platform. Then, the
111 LAWSD30 dataset was employed to evaluate and recognize the spatiotemporal variations in SD
112 for lakes with areas $> 0.01 \text{ km}^2$ ($N = 40,973$) across China in the period 1985–2020. Our results
113 can provide effective data support for the management and protection of lake water
114 environment.

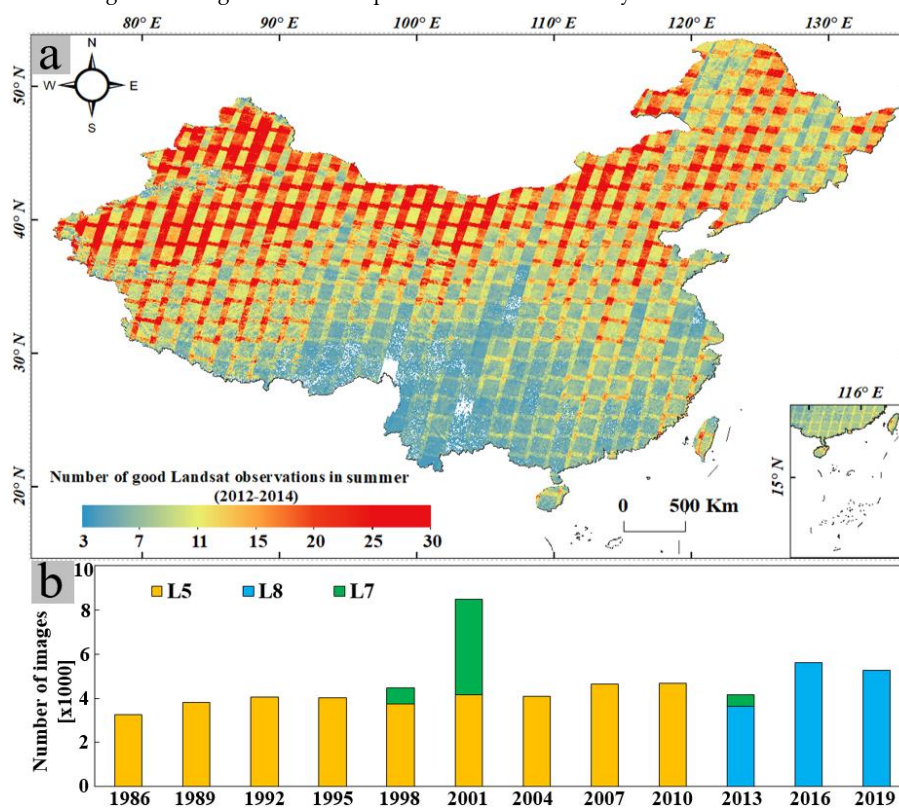
115 2. Datasets

116 2.1. Landsat series satellite datasets

117 Taking into account the frequent contamination of cloud and cloud shadow, it is hard to
118 develop a spatially continuous product throughout China with only one year of Landsat images
119 (Zhang et al., 2019a). Therefore, we used images from ± 1 year of the target year to generate each
120 product, and a total of 12 SD products with a three-year time step were developed for 1985–
121 2020. All available Landsat series Level-1 precision terrain (L1TP) surface reflectance datasets
122 (about 46 terabytes of data), including Landsat 5 Thematic Mapper (TM), Landsat 7 Enhanced
123 Thematic Mapper-plus (ETM+), and Landsat 8 Operational Land Imager (OLI) imagery,
124 acquired in the summer (June 1–September 30) from 1985 to 2020, were used via the GEE cloud
125 computing platform. The summer months were chosen because the water clarity is relatively
126 stable in this season and suitable for monitoring with remote sensing imagery (Kloiber et al.,
127 2002; Mccullough et al., 2012; Singh and Singh, 2015; Song et al., 2020). In addition, since the



128 Landsat L1TP data were intercalibrated across different Landsat series sensors, the collected
129 L1TP data were consistent and suitable for pixel-level time series analysis (Racetin et al., 2020).
130 However, since the Landsat 7 scan line corrector (SLC) failed in 2003, the Landsat 7 images
131 acquired thereafter exhibited wedge-shaped scan gaps (referred to as SLC-off images) (Usgs,
132 2003). Therefore, except for 2012–2014, only Landsat 7 data before 2003 were used for the
133 development of our SD products (Fig. 1b). Since Landsat 5 retired in 2011 and Landsat 8 data
134 were only available after 2013, the valid Landsat observations from 2012 to 2014 were
135 insufficient (Fig. 1a). Therefore, a few Landsat 7 SLC-off images from 2012 to 2014 were used as
136 substitutes to fill the gaps between 2012 and 2014. Fig. 1b shows the final number of Landsat
137 series images used to generate the SD product for each nominal year.



138
139 **Figure 1.** Valid Landsat 5 and 8 observations in China from 2012 to 2014 (a) and statistics of Landsat images
140 used to develop the product for each nominal year (b). Note: L8., Landsat 8; L7., Landsat 7; L5., Landsat 5.

141 2.2. Auxiliary inland water products

142 The annual 30 m Joint Research Centre Global Surface Water (JRC-GSW) database was used
143 to extract water body regions for each SD product (Pekel et al., 2016). The JRC-GSW was
144 developed based on multiple classification criteria and time-series Landsat 5, 7, and 8 data from
145 1984 to 2019, and archived to the GEE platform. The water pixels in the JRC-GSW were labeled
146 as permanent and seasonal water pixels based on the frequency of being detected as water
147 bodies (Pekel et al., 2016). The overall user and producer accuracies for permanent water were
148 99.6% and 98.6%, respectively, versus 98.6% and 75.4% for seasonal water (Pekel et al., 2016).

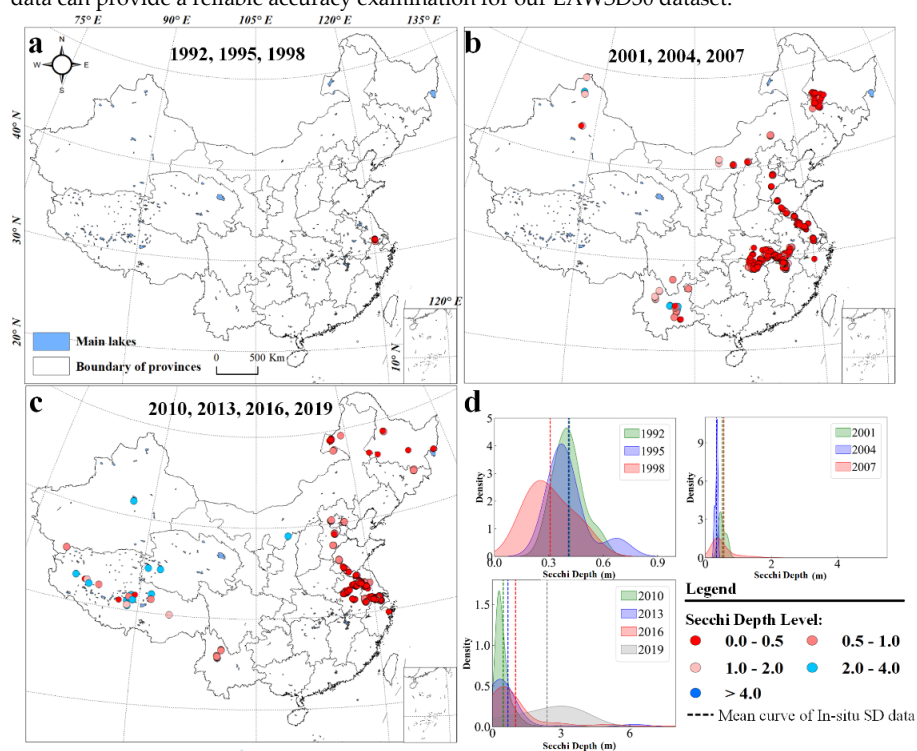


149 Following Chen et al. (2021), in this study, only the pixels marked as permanent waters in the
150 JRC-GSW were utilized to extract water regions to reduce the disturbance from aquatic
151 vegetation in seasonal waters.

152 Additionally, the existing Chinese lake inventories (Ma et al., 2011; Song et al., 2020; Chen
153 et al., 2021) and the Reservoirs and Dams vector database (Song et al., 2018) were also collected
154 and used to extract lakes for each SD product.

155 2.3. In situ SD datasets

156 In order to quantitatively evaluate the performance of the LAWS30 dataset, a total of 1502
157 in situ SD measurements of 208 lakes between 1992 and 2019 were collected from the China Lake
158 Scientific Database (<http://www.lakesci.csdb.cn>), the National Earth System Science Data Center,
159 National Science & Technology Infrastructure of China (<http://lake.geodata.cn>), and work by
160 Wang et al. (2020) and Liu et al. (2020). Due to the scarcity of field-measured SD records before
161 the 1990s, only SD products after 1992 were validated. Since in situ SD measurements within
162 seven days of satellite overpasses were suitable for the validation of the remote-sensing-derived
163 SD product (Song et al., 2020), the collected SD measurements were coincident with the Landsat
164 data used in our study within a window of ± 7 days. The distributions of the in situ SD records
165 collected to validate products for different nominal years are shown in Fig. 2a–c. The probability
166 density of the collected SD measurements used for each SD product was calculated and is
167 exhibited in Fig. 2d. It can be seen that the collected SD measurements cover a variety of water
168 clarity conditions and are distributed throughout China (Fig. 2). The values of our collected SD
169 data range from 0 to 7 m, covering lakes from clear to eutrophic. Therefore, the collected in situ
170 data can provide a reliable accuracy examination for our LAWS30 dataset.



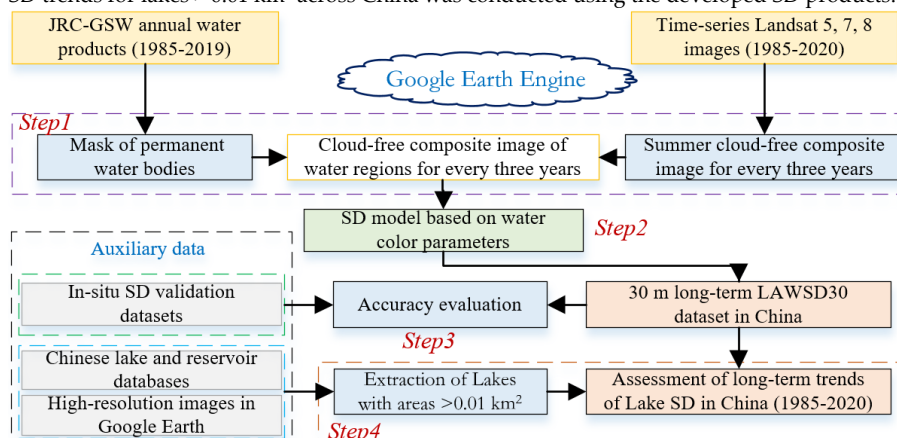
171



172 **Figure 2.** Details of the in situ measured SD datasets. (a–c) The geographical distributions of SD samples
 173 used to validate the accuracies of the corresponding SD products; (d) the probability density of the
 174 collected SD measurements used for each target SD product, used to show the SD range where the collected
 175 in situ SDs are mainly concentrated.

176 3. Methodology

177 In order to assess the long-term trends of SD in Chinese lakes, four steps were taken in our
 178 study (Fig. 3). First, based on the time-series Landsat images and the JRC-GSW water products
 179 archived in GEE, a summer cloud-free composite image was generated between 1985 and 2020
 180 with an interval of three years using the best-available-pixel (BAP) compositing method. Then,
 181 based on the generated cloud-free composite images, the long-term LAWS30 dataset from
 182 1985 to 2020 (including 12 products, representing 1986, 1989, 1992, 1995, 1998, 2001, 2004, 2007,
 183 2010, 2013, 2016, and 2019) were developed using a robust SD model based on water color
 184 parameters. Next, the accuracy of our developed LAWS30 dataset was evaluated using the
 185 collected concurrent in situ datasets. Finally, with the assistance of the existing Chinese lake and
 186 reservoir datasets and high-resolution images in Google Earth, the assessment of the long-term
 187 SD trends for lakes $> 0.01 \text{ km}^2$ across China was conducted using the developed SD products.



188 **Figure 3.** A flowchart of the long-term LAWS30 dataset development steps and the long-term SD trend
 189 assessment of lakes in China. Note: LAWS30, 30 m LAKE Water SD dataset of China.
 190

191 3.1. Generation of cloud-free composites using best-available-pixel (BAP) composition method

192 Since summer is suitable for SD mapping with remote sensing imagery (McCullough et al.,
 193 2012; Singh and Singh, 2015; Song et al., 2020), cloud-free summer composites of Landsat data
 194 for 12 three-year time steps were compiled from 1985 to 2010. Generally, the median and mean
 195 composite methods were used to generate cloud-free images in the SD assessing studies (Li et
 196 al., 2020a; Wang et al., 2020; Liu et al., 2020). However, since multisource sensors (TM, ETM+,
 197 and OLI) were used in this study, the different band settings between these sensors made the
 198 parameters of the algorithm specific to each sensor (Li et al., 2020a; Garnesson et al., 2019).
 199 Because the median and mean composite methods will change the original radiation value of
 200 the pixel (Xie et al., 2019; Griffiths et al., 2014), the composite pixels derived from these general
 201 methods are difficult to trace back to the sensor from which they originated. Therefore, these
 202 methods are not well suitable for our research. Recently, White et al. (2014) proposed a BAP



203 method to generate cloudless composites on a large area. Since BAP compiles cloud-free images
204 by selecting the best available observation based on user-defined criteria (Gomez et al., 2016;
205 Griffiths et al., 2013), the BAP composites can retain the source image information from which
206 they came. In addition, since BAP can ensure phenological consistency between multitemporal
207 BAP composites by setting the acquisition day-of-year (DOY) criteria (Griffiths et al., 2014; Chen
208 et al., 2021), it is suitable for multiyear change detection and assessment (Griffiths et al., 2014;
209 Gomez et al., 2016; Hermosilla et al., 2015; Zhang et al., 2021a). Accordingly, the BAP method
210 was used to generate cloud-free composites. Our team recently used BAP to develop summer
211 composites for water color mapping (Chen et al., 2021). Following him, the DOY criteria, the
212 cloud and cloud shadow criteria, and the atmospheric opacity criteria were selected to generate
213 the BAP composites. The score for each criterion was summed, and the observation with the
214 highest score was selected as the BAP composite. The parameter values for the criteria used were
215 obtained from Chen et al. (2021).

216 However, since floods and rainfall in summer will bring suspended particles into water
217 bodies, making the SD of water bodies much lower than usual (Murshed et al., 2014; Liu et al.,
218 2021), it is also necessary to reduce the impact of these factors on the BAP composites to ensure
219 the reliability of the long-term SD trend assessment. Here, the normalized difference turbidity
220 index (NDTI) (Lacaux et al., 2007) was used to indicate the turbidity of the water (Eq. (1)). As
221 the SD of water decreases, the NDTI of water increases (Islam, 2006; Lacaux et al., 2007).
222 Therefore, the interference of floods and rainfall was restricted by only using the observations
223 with NDTI less than the 80th quantile of their NDTI stack for BAP compositing.

$$NDTI = (Red - Green)/(Red + Green) \quad (1)$$

224 Finally, based on the intra-annual permanent water pixels detected in the JRC-GSW, water
225 regions were extracted from the BAP composites.

226 3.2. Inversion model of water SD

227 Previous studies have proven that FUI and hue angle (α) are useful water color parameters
228 for assessing the SD of inland waters (Wang et al., 2020; Chen et al., 2021; Garaba et al., 2015).
229 Recently, these two watercolor parameters were further demonstrated to be robust parameters
230 for retrieving SD over large areas and long-term spans (Wang et al., 2020; Pitarch et al., 2019).
231 Therefore, the SD of the extracted permanent water regions was retrieved using a robust SD
232 model based on FUI and α (Wang et al., 2020). The SD model showed good performance and
233 adaptability over a variety of water clarity ranges, with a mean relative difference of 27.4% and
234 a mean absolute difference of 0.37 m (Wang et al., 2020). There are three main steps in the SD
235 model:

236 (1) *Calculation of the hue angle (α):* The α is the angle of the line drawn anti-clockwise from
237 the positive x-axis at $y = 1/3$ in the Commission on Illumination's (CIE) chromaticity diagram
238 (Wang et al., 2018). In order to derive the angle α , the CIE primary color tristimulus (X, Y, Z)
239 was calculated from the reflectance in the visible bands of Landsat images first (Wang et al., 2020;
240 Chen et al., 2021). Since ETM+/TM has only three bands in the visible range, the tristimulus of
241 Landsat ETM+/TM was calculated using the RGB conversion method (Wang, 2018; Cie, 1932)
242 (Eqs. (2)-(4)):

$$X = 1.1302 R(485) + 1.7517 R(565) + 2.7689 R(660) \quad (2)$$

$$Y = 0.0601 R(485) + 4.5907 R(565) + 1.0000 R(660) \quad (3)$$



$$Z = 5.5943 R(485) + 0.0560 R(565), \quad (4)$$

243 where R represents the band reflectance. Since OLI has four visible bands, the X , Y , and Z of
 244 Landsat OLI data were calculated using the linear weighted summation method as per Chen et
 245 al. (2021) (Eqs. (5)–(7)):

$$X = 11.053 R(443) + 6.950 R(482) + 51.135 R(561) + 34.457 R(655) \quad (5)$$

$$Y = 1.320 R(443) + 21.053 R(482) + 66.023 R(561) + 18.034 R(655) \quad (6)$$

$$Z = 58.038 R(443) + 34.931 R(482) + 2.606 R(561) + 0.016 R(655). \quad (7)$$

246 Once the tristimulus was calculated, the chromaticity coordinates (x , y) were then acquired from
 247 the X , Y , and Z (Wang et al., 2021) (Eq. (8)). Afterwards, the hue angle α was derived based on x
 248 and y (Van Der Woerd and Wernand, 2018) (Eq. (9)). However, because of the band settings of
 249 sensors, there is an offset ($\Delta\alpha$) of the sensor-derived hue angle (Van Der Woerd and Wernand,
 250 2015). Following the ideas in Van Der Woerd and Wernand (2015), Wang (2018) recently
 251 developed polynomial deviation delta corrections for multiple sensors (Eq. (10)). Accordingly,
 252 the angle α was finally corrected using $\alpha + \Delta\alpha$.

$$x = X/(X + Y + Z), \quad y = Y/(X + Y + Z) \quad (8)$$

$$\alpha = \text{ARCTAN2}\left(y - \frac{1}{3}\right) / \left(x - \frac{1}{3}\right) * 180/\pi \quad (9)$$

$$\Delta\alpha = a(\alpha/100)^5 + b(\alpha/100)^4 + c(\alpha/100)^3 + d(\alpha/100)^2 + e\left(\frac{\alpha}{100}\right) + f, \quad (10)$$

253 where a – f are coefficients of the deviation delta correction, and the correction coefficients of
 254 OLI/ETM+/TM are shown in Table 1.

255 **Table 1.** Polynomial coefficients for the Landsat-OLI/TM/ETM+ hue angle correction (Wang, 2018).

Sensor	a	b	c	d	e	f
Landsat-TM	25.851	-177.4	476.69	-653.3	463.33	-94.41
Landsat-ETM+	30.473	-203.4	498.8	-570.9	324.73	-56.72
Landsat-OLI	21.355	-199.29	703.3	-1132.2	801.6	-201.34

256 (2) *Calculation of the FUI:* The FUI for pixels in Landsat were derived from the corrected
 257 angle α based on the FUI lookup table (Novoa et al., 2013) (Table 2). Each FUI corresponds to a
 258 range of angle α .

259 **Table 2.** The 21-class FUI indices and the corresponding range of hue angle α (Wang et al., 2018; Chen et
 260 al., 2021).

FUI	α range (°)	FUI	α range (°)	FUI	α range (°)
1	(35.00, 42.83)	8	(160.97, 175.98)	15	(219.34, 224.87)
2	(42.83, 49.02)	9	(175.98, 186.67)	16	(224.87, 230.23)
3	(49.02, 60.01)	10	(186.67, 195.44)	17	(230.23, 235.09)
4	(60.01, 79.23)	11	(195.44, 202.05)	18	(235.09, 239.56)
5	(79.23, 106.94)	12	(202.05, 207.82)	19	(239.56, 243.66)
6	(106.94, 137.03)	13	(207.82, 213.57)	20	(243.66, 247.25)
7	(137.03, 160.97)	14	(213.57, 219.34)	21	(247.25, 252.00)

261 (3) *Calculation of the SD:* Based on the calculated FUI and α , the SD was obtained following
 262 the algorithm proposed in Wang et al. (2020) (Eqs. (11)–(12)). This model had been proved to be
 263 suitable for large-area and long-term SD monitoring (Wang et al., 2020).

$$\text{FUI} < 8, \text{SD} = 794630.86 \cdot \alpha^{-1.66} \quad (11)$$



$$FUI \geq 8, SD = 30380 \cdot FUI^{-2.621} \quad (12)$$

264 3.3. Assessment of long-term SD trends in China's Lakes

265 In order to comprehensively evaluate the long-term trends in SD of natural lakes across
266 China, lakes with areas $> 0.01 \text{ km}^2$ (more than 10 pixels) were manually extracted by referring
267 to the Chinese lake inventories (Chen et al., 2021; Song et al., 2020), the Chinese reservoir and
268 dam database (Song et al., 2018), and high-resolution images from Google Earth. Since previous
269 water investigations were mainly based on MODIS and Sentinel-3 images, and focused on lakes
270 with an area $> 1 \text{ km}^2$, the knowledge of lakes $< 1 \text{ km}^2$ was limited (Zhang et al., 2021b; Chen et
271 al., 2021). Therefore, in our study, the extracted lakes were divided into two groups, lakes with
272 an area $> 1 \text{ km}^2$ and lakes with an area $\leq 1 \text{ km}^2$, to explore the SD trends in the two different
273 areas. In order to reduce the impact of aquatic vegetation, algae bloom areas, and shallow
274 nearshore on the lake SD assessment, the mean SD of each lake was calculated following the
275 method in Chen et al. (2021). Specifically, the floating algae index (FAI) (Eq. (13)) (Dai et al., 2021;
276 Hu, 2009) was first used to mask algae bloom and aquatic vegetation areas with a threshold of
277 -0.02 (Chen et al., 2021). Then, shallow near-shore pixels were excluded by setting the
278 corresponding threshold value for each lake (Chen et al., 2021). Pixels whose SD was less than
279 the SD value of 80% of the pixels in a given lake were regarded as shallow near-shore pixels and
280 excluded. After the above steps, the remaining pixels in each lake region were used to calculate
281 the mean SD of that lake as follows:

$$FAI = NIR - (Red + (SWIR - Red) \times (\lambda_{NIR} - \lambda_{Red}) / (\lambda_{SWIR} - \lambda_{Red})), \quad (13)$$

282 where Red, NIR, and SWIR represent the reflectance of red, near-infrared (NIR), and shortwave
283 infrared (SWIR) bands, and λ_{NIR} , λ_{Red} , and λ_{SWIR} are the center wavelengths of NIR, red, and
284 SWIR bands.

285 The nonparametric Loess regression method (Steyerberg, 2016) was employed to delineate
286 the long-term SD trend for each lake, and the widely used Mann–Kendall (MK) test (Yuan et al.,
287 2018; Kendall, 1990; Mann, 1945) was applied to indicate the monotonicity of the long-term SD
288 trend. Specifically, the MK indicated the monotonic trend by using a standardized MK statistic
289 Z (Yuan et al., 2018). $Z > 0$ indicated an upward trend, while $Z < 0$ indicated a downward trend.
290 The indicated trend was regarded as significant only when $P \leq 0.05$ (Li et al., 2020a). Since the
291 reliability of the long-term trend analysis relied on the observation number of time series data
292 (Li et al., 2020a; Wang et al., 2020), only the lakes that existed in at least 10 SD products were
293 retained for our long-term SD assessment. Using the above criteria, a total of 40,973 lakes were
294 used for time series SD analysis.

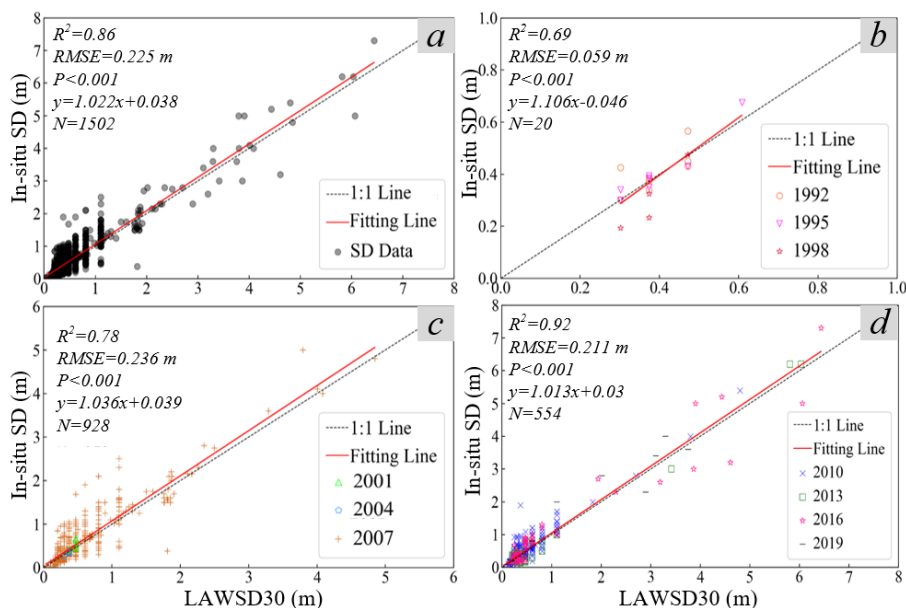
295 4. Results

296 4.1. Accuracy evaluation of the 30 m long-term LAWS30 dataset

297 The accuracy of our LAWS30 dataset was evaluated with the collected concurrent in situ
298 SD datasets, as illustrated in Fig. 4. From Fig. 4a, our LAWS30 dataset exhibited a significant
299 correlation with all collected in situ SD data, with an R^2 of 0.86 and an $RMSE$ of 0.225 m. Most
300 of the scatter points were distributed close to the 1:1 line. Specifically, from the validation results
301 in the 2010s, our LAWS30 showed good performance, with an R^2 of 0.92 and an $RMSE$ of 0.211



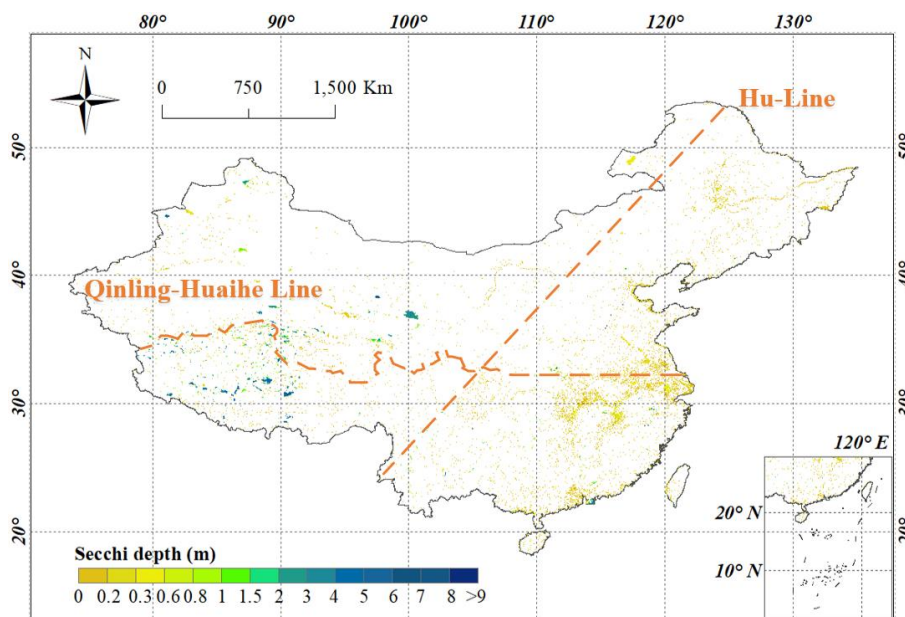
302 m. In addition, a stable performance was also shown in the results for the 2000s, with R^2 reaching
303 0.78 and $RMSE$ reaching 0.236 m. Furthermore, a good performance was also seen before the
304 2000s, with an R^2 of 0.69 and an $RMSE$ of 0.059 m in the 1990s. The validation results for these
305 different decades proved the stable performance of our LAWS30 in different periods. It is
306 concluded, therefore, that our LAWS30 can be a reliable dataset for the long-term SD trend
307 assessment of lakes in China.



308 **Figure 4.** Scatterplots of the in situ measured SD data and our LAWS30 dataset. (a) An overall scatterplot
309 of our LAWS30 dataset and all the collected in-situ SD data; (b–d) scatterplots of our LAWS30 dataset
310 and the corresponding in situ SD data in the 1990s (1992, 1995, and 1998), 2000s (2001, 2004, and 2007), and
311 2010s (2010, 2013, 2016 and 2019), respectively.
312

313 4.2. The LAWS30 dataset in China

314 Our developed long-term LAWS30 dataset includes 12 SD products of the corresponding
315 nominal years, now available at <https://doi.org/10.5281/zenodo.5734071>. Here, the SD product
316 in 2019 is shown in Fig. 5. It can be found that the water bodies in our product showed a wide
317 range of SD values (0.1 m to more than 9 m), indicating a great diversity of Chinese inland waters.
318 Taking the famous Hu line (Hu, 1990) as the boundary, the SD of water bodies showed an
319 obvious pattern of “high west and low east” across China. The average SD of the water bodies
320 to the west of the Hu line was approximately 1.7 m, while the average SD of the eastern water
321 bodies was about 0.4 m. Furthermore, regarding the famous Qinlin–Huaihe line (Liu et al., 2015),
322 the dividing line between the north and south of China, a significant latitudinal pattern of “high
323 in the south and low in the north” was exhibited across China. The average SD of the water
324 bodies distributed to the north of the Qinlin–Huaihe line was about 0.72, whereas the average
325 SD reached about 1.16 for the water bodies south of this line. The above SD patterns observed
326 across China were in good agreement with other studies (Wang et al., 2020; Zhang et al., 2021b).



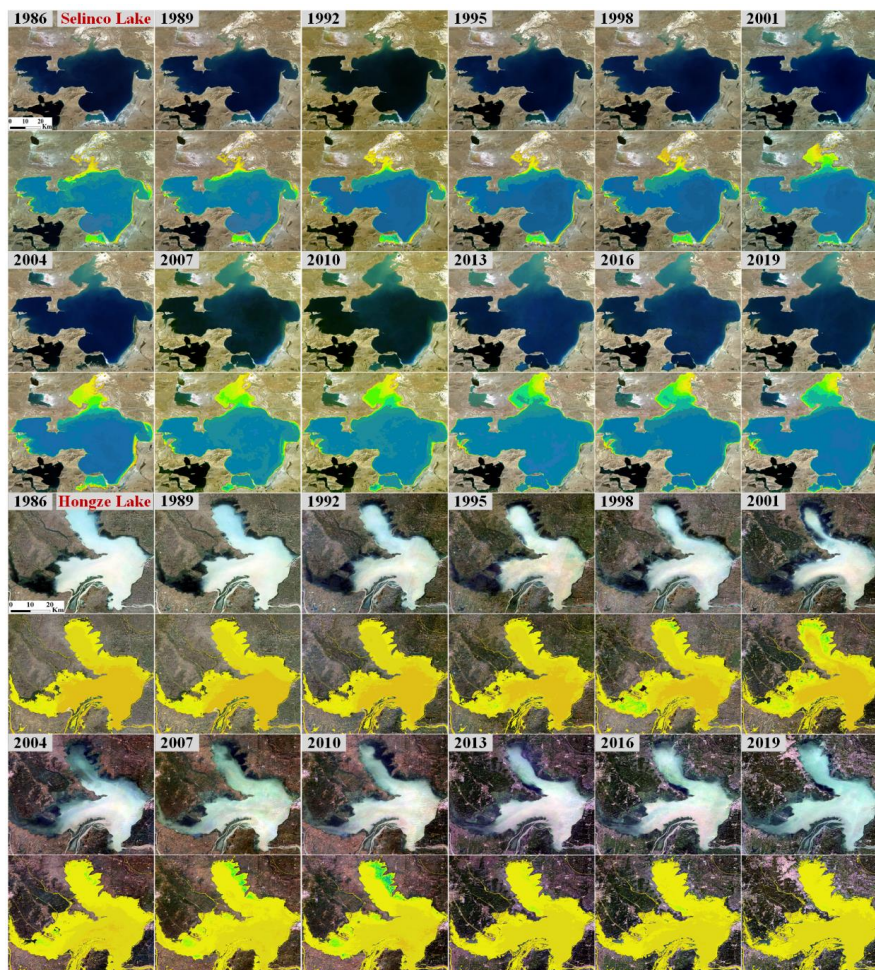
327

328 **Figure 5.** The 30 m SD product in China in 2019. Note: the north–south dashed line is the Hu line, and the
329 east–west dashed line is the Qinling–Huaihe Line.

330 Moreover, in order to illustrate the ability of our long-term LAWS30 dataset to monitor
331 the spatiotemporal pattern of SD in water bodies, the time-series SD results for two important
332 lakes, Selinco Lake and Hongze Lake, are displayed and used as case studies (Fig. 6). The long-
333 term mean SD of the two lakes is shown in Fig. 7. From the perspective of the spatial pattern, it
334 can be seen that the water area in the northern part of Selinco Lake has been increasing, and the
335 SD of the north is generally lower than that of the central and southern areas of the lake. A
336 significant pattern of “high center and low north” was found from the SD results for Selinco
337 Lake. Additionally, an obvious clarity gradient with high values on the northern side and lower
338 values on the central area and southern side could be found in Hongze Lake. These results are
339 in good agreement with previous researches (Wang et al., 2020; Xue et al., 2019; Liu et al., 2021).
340 Furthermore, we can see that the clarity of water in the northern part of Selinco Lake has
341 improved in recent years, and the SD in the central and southern regions of Hongze Lake has
342 also increased compared with 35 years ago (Fig. 6). Moreover, in terms of the SD trends, the
343 mean SD of Selinco Lake exhibited a decreasing but insignificant trend ($Z < 0$, $P > 0.05$) in the
344 period 1985–2020, while Hongze Lake has shown a significant, increasing SD trend ($Z > 0$, $P <$
345 0.05) over the past 35 years (Fig. 7). Specifically, the SD curve of Selinco Lake first showed an
346 upward trend before the 2000s, and then exhibited a decreasing trend after 2001. As for Hongze
347 Lake, it was found to have an increasing SD trend before 2010, but the SD began to decrease
348 after that. Similarly, some studies found the same SD change patterns in the two lakes (Liu et
349 al., 2021; Li et al., 2016; Wang et al., 2020; Zhigang et al., 2017; Li et al., 2019). Therefore, our
350 long-term SD dataset can provide an opportunity to quickly evaluate the temporal dynamics of
351 SD in water bodies at low cost, which is of great significance for large-scale water quality



352 monitoring.

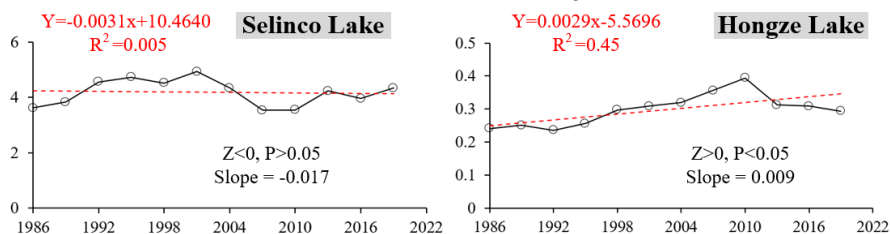


353

354

355

Figure 6. The long-term SD results of Selinco Lake and Hongze Lake between 1985 and 2020. Note: the color bar is the same as that in Fig. 5.



356

357

Figure 7. The long-term SD curves of Selinco Lake and Hongze Lake.

358

4.3. Long-term SD trend of lakes across China in the period 1985–2020

359

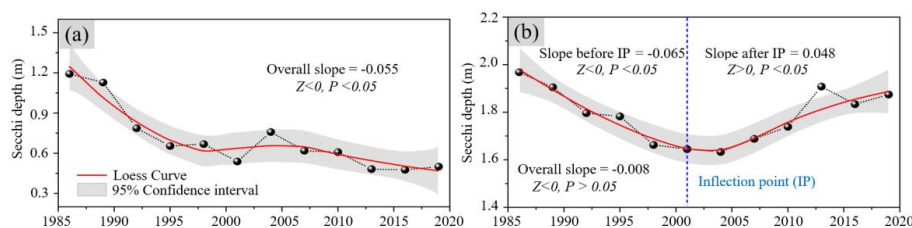
360

361

The long-term variations in SD for lakes with an area $> 0.01 \text{ km}^2$ ($N = 40,973$) across China from 1985 to 2020 were first evaluated and recognized using our LAUSD30 products (Fig. 8). First, for lakes with an area $\leq 1 \text{ km}^2$ (Fig. 8a), the mean SD of the lakes showed a significant



362 downward trend since 1985 ($Z < 0$, $P < 0.05$), with a rate of -0.055 m/year. However, it can be
363 seen that the decline rate of SD began to slow down and stabilized after 2001 (with a rate of $-$
364 0.026 m/year after 2001). In addition, regarding lakes with areas > 1 km² (Fig. 8b), the mean SD
365 of the lakes around 2020 was basically the same as that in 1985, and the long-term SD of the
366 lakes has not shown a significant downward trend since 1985 ($Z < 0$, $P > 0.05$). However, by
367 carefully observing the time series SD curve of these lakes (Fig. 8b), an obvious turning point
368 could be found around 2001. The SD of the lakes showed a significant downward trend ($Z < 0$,
369 $P < 0.05$) before 2001, and began to increase significantly ($Z > 0$, $P < 0.05$) afterward. The above
370 results demonstrate that the water clarity of lakes in China has continued to improve since the
371 21st century, but the SD of lakes with an area ≤ 1 km² is still low.



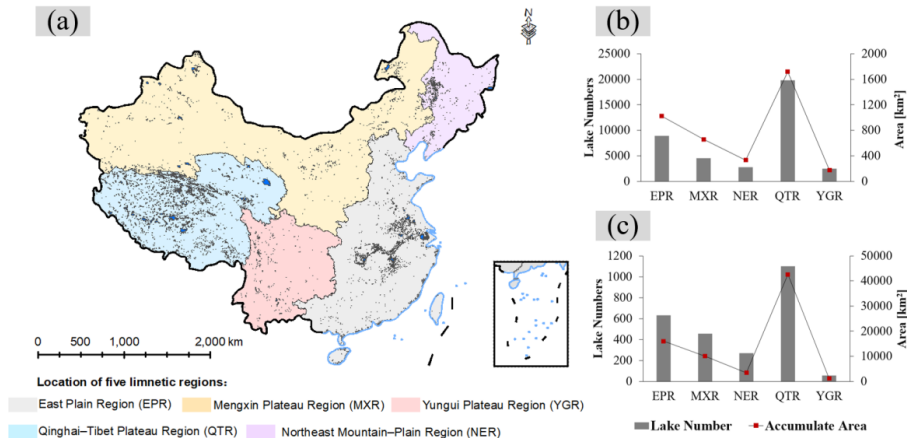
372
373 **Figure 8.** The long-term trend in SD for lakes with an area > 0.01 km² ($N = 40,973$) across China from 1985
374 to 2020. (a) The mean SD of lakes ≤ 1 km² across China; (b) the mean SD of lakes > 1 km² across China. Note:
375 IP., inflection point.

376 In order to further evaluate the long-term SD trends of lakes in different geographic regions,
377 China was divided into five limnetic regions (Ma et al., 2011; Chen et al., 2021), i.e., the Northeast
378 Mountain Plain Region (NER), Eastern Plain Region (EPR), Yunnan–Guizhou Plateau Region
379 (YGR), Qinghai–Tibet Plateau Region (QTR), and Mongolian–Xinjiang Plateau Region (MXR)
380 (Fig. 9). The statistics of lakes with an area > 1 km² and an area ≤ 1 km² are shown in Fig. 9b and
381 Fig. 9c, respectively. It can be seen that the number of lakes with an area ≤ 1 km² in each region
382 was far greater than that of lakes with an area > 1 km², but their accumulation area was much
383 smaller than that of lakes with an area > 1 km². Furthermore, the number and area of lakes in
384 QTR were the highest, while those in YGR were the lowest.

385 Fig. 10 gives the long-term SD trend of lakes in each limnetic region. For lakes ≤ 1 km² (Fig.
386 10a–e), it can be seen that, except for MXR and QTR, the SD of the lakes in other regions did not
387 show a significant decreasing trend ($P > 0.05$) during the entire analysis period. Moreover, the
388 SD of small lakes (area ≤ 1 km²) in EPR and NER showed obvious increases ($Z > 0$, $P < 0.05$) since
389 1985, with average change rates of 0.015 m/year and 0.005 m/year, respectively. Although the
390 SD of small lakes in MXR and QTR experienced significant downward trends over the past 35
391 years, the decline rates slowed down after the beginning of the 21st century (with rates of 0.001
392 m/year in MXR and -0.045 m/year in QTR after 2001), and the decrease trend had not been
393 significant since 2001 ($Z < 0$, $P > 0.05$). Secondly, as for lakes > 1 km², there were no dramatic
394 decreases in SD in any of the five regions from 1985 to 2020. Moreover, the lakes with an area $>$
395 1 km² in NER experienced a significant upward trend in water clarity ($Z > 0$, $P < 0.05$) over the
396 past 35 years. Additionally, we can also see that the water clarity of lakes > 1 km² in MXR and
397 QTR significantly improved since the beginning of the 21st century. The SD of lakes > 1 km² in
398 YGR in 2020 was also higher than that in 1985. However, it should be noted that, although the
399 SD of lakes > 1 km² in 2020 was also greater than that in 1985 in EPR, the SD of these lakes was

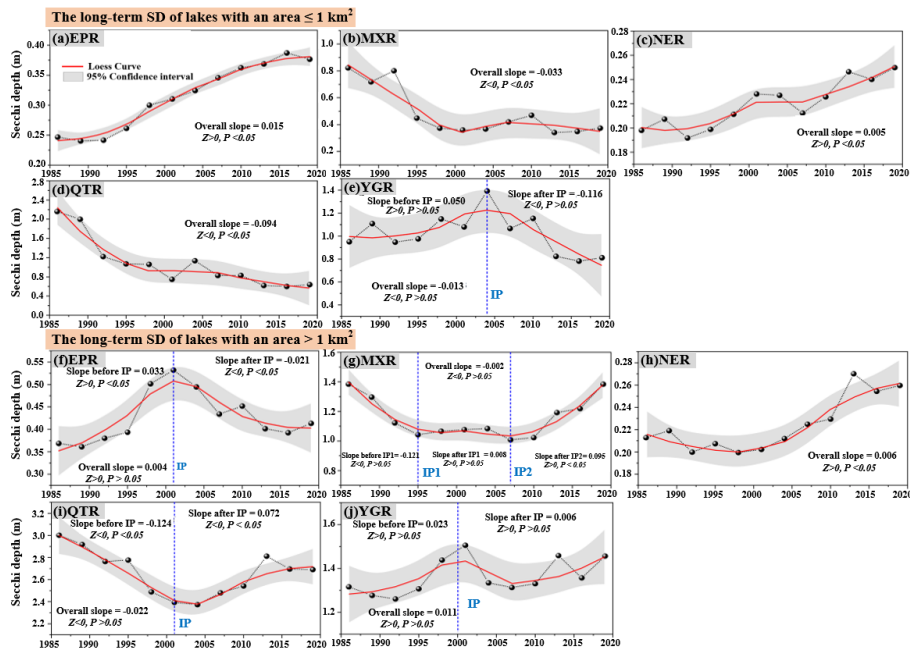


400 characterized by a significant decrease, with a rate of -0.021 m/year after 2001.



401

402 **Figure 9.** The location of the five limnetic regions and the lake statistics in each limnetic region. (a) The
 403 location of the five limnetic regions; (b) statistics of lakes with areas ≤ 1 km² in each region; (c) statistics of
 404 lakes with areas > 1 km² in each region.



405

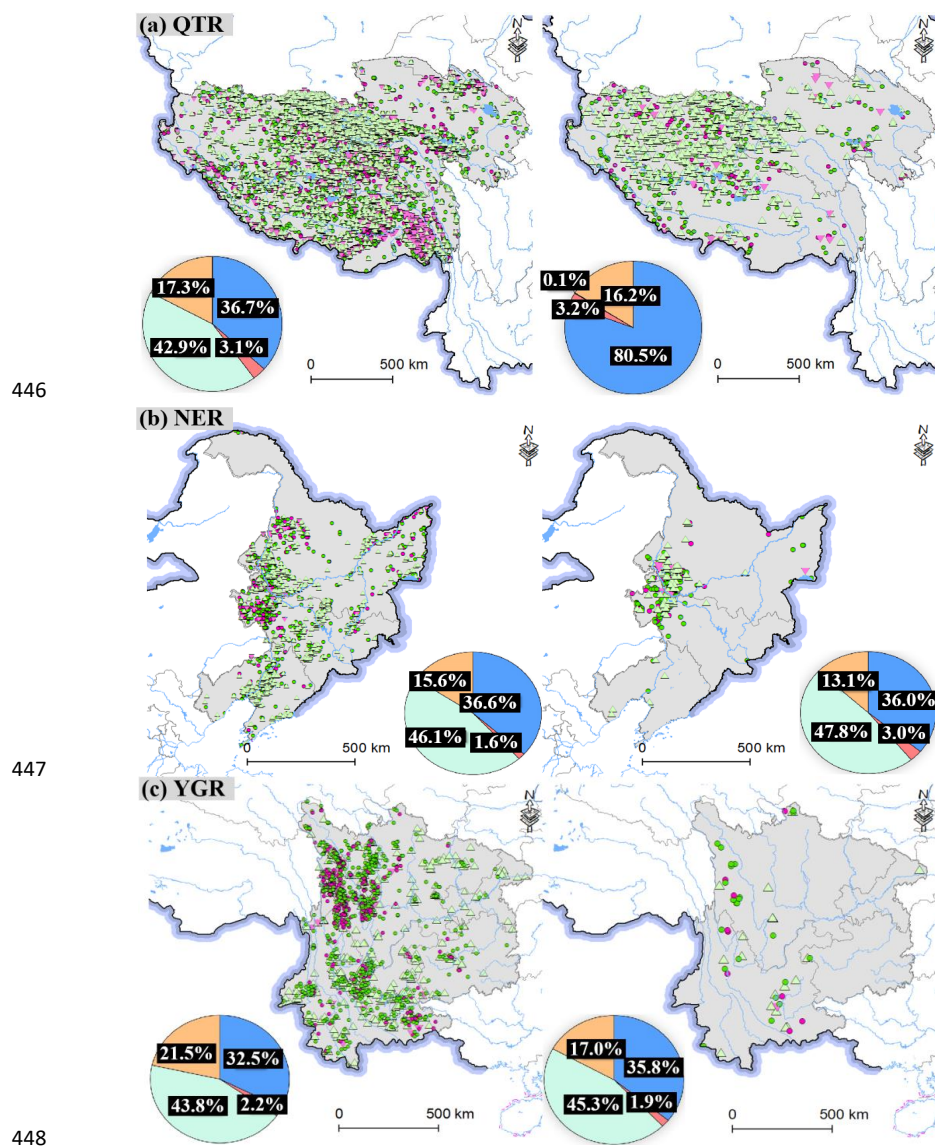
406 **Figure 10.** The long-term SD trend of lakes in each limnetic region from 1985 to 2020. (a–e) The long-term
 407 SD trend of lakes with an area ≤ 1 km² in each region; (f–j) the long-term SD trend of lakes with an area $>$
 408 1 km² in each region. Note: EPR., Eastern Plain Region; MXR., Mongolian-Xinjiang Plateau Region; NER.,
 409 Northeast Mountain Plain Region; QTR., Qinghai-Tibet Plateau Region; YGR., Yunnan-Guizhou Plateau
 410 Region; IP., inflection point.

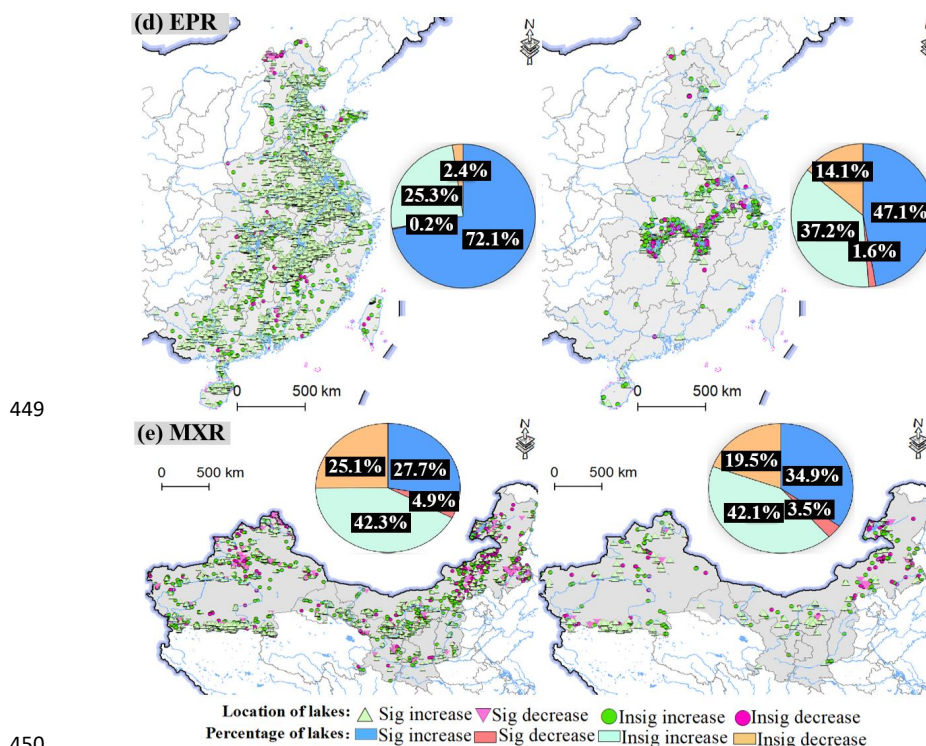
411 4.4 Spatiotemporal patterns of water clarity in lakes over China



412 The spatiotemporal patterns of SD in lakes in the five limnetic regions from 1985 to 2020 are
413 shown in Fig. 11. Overall, for lakes with an area $\leq 1 \text{ km}^2$ and $> 1 \text{ km}^2$, the average proportions of
414 lakes with an increasing SD trend were about 76.1% and 81.3%, respectively, in the five limnetic
415 regions. In addition, the region with the lowest percentage of lakes tending to become clear
416 (with an increasing trend) was still about 70.0%. The above results indicate that most lakes in
417 China exhibited a tendency to become clear in the period 1985–2020. Specifically, as for lakes
418 with areas $\leq 1 \text{ km}^2$ (hereinafter referred to as small lakes), the minimum proportion of small
419 lakes whose SD was characterized by an increasing trend was in the MXR (about 70.0%), while
420 the maximum proportion appeared in the EPR (about 97.4%). In addition, for lakes with areas $>$
421 1 km^2 (hereinafter referred to as large lakes), the smallest and largest proportions of large lakes
422 that had increasing trends were also in the MXR (about 77.0%) and the EPR (about 84.3%),
423 respectively.

424 Focusing on the detailed spatial–temporal SD patterns in each limnetic region, there were
425 basically no small lakes with a decreasing trend in SD (2.6%) in the EPR. The individual small
426 lakes that experienced downward trends in EPR were mainly located at the northernmost
427 regions and at the junction of Hubei and Hunan Provinces. Moreover, as for the large lakes in
428 the EPR, these were mainly distributed along the Yangtze River, and the lakes showing
429 decreasing SD trends were mainly located in the middle reaches of the Yangtze River. Secondly,
430 the MXR was the region with the minimum percentage of lakes that had an increasing trend
431 among the five limnetic regions. Specifically, small lakes that exhibited decreasing trends were
432 mainly located in the northeast and northwest of MXR, while large lakes that had decreasing
433 trends were mainly distributed in the northeast areas of MXR. Additionally, in the NER, large
434 and small lakes with decreasing SD were mainly distributed in the west and northeast of NER,
435 accounting for 17.2% of small lakes and 16.1% of large lakes, respectively. Furthermore, in the
436 QTR, most lakes were located in the north, center, and southeast. Among these lakes, most of
437 the small lakes with a tendency to become turbid were located in the center, northeast, and
438 southeast of QTR. In addition, the large lakes that were characterized by decreasing trends were
439 mainly distributed in the central and northeast parts of the QTR. Lastly, as for the lakes in YGR,
440 the small lakes that had a decreasing trend were mainly located in the northwest and southeast
441 of YGR. In contrast, the number of large lakes in the YGR was relatively small ($N = 53$), and the
442 lakes with a decreasing trend were mainly distributed in the southeast and west of YGR.
443 Therefore, although most lakes had a tendency to become clearer from 1985 to 2020, there was
444 still a considerable proportion of lakes whose SD experienced a downward trend over the past
445 few decades, which suggests that effective water management is still required in many regions.





450
 451 **Figure 11.** The spatiotemporal patterns of SD in lakes in the five limnetic regions from 1985 to 2020 (from
 452 left to right are the spatiotemporal patterns of lakes with an area $\leq 1 \text{ km}^2$, and the spatiotemporal patterns
 453 of lakes with an area $> 1 \text{ km}^2$). Note: Sig., significant; Insig., insignificant.

454 **5. Discussion**

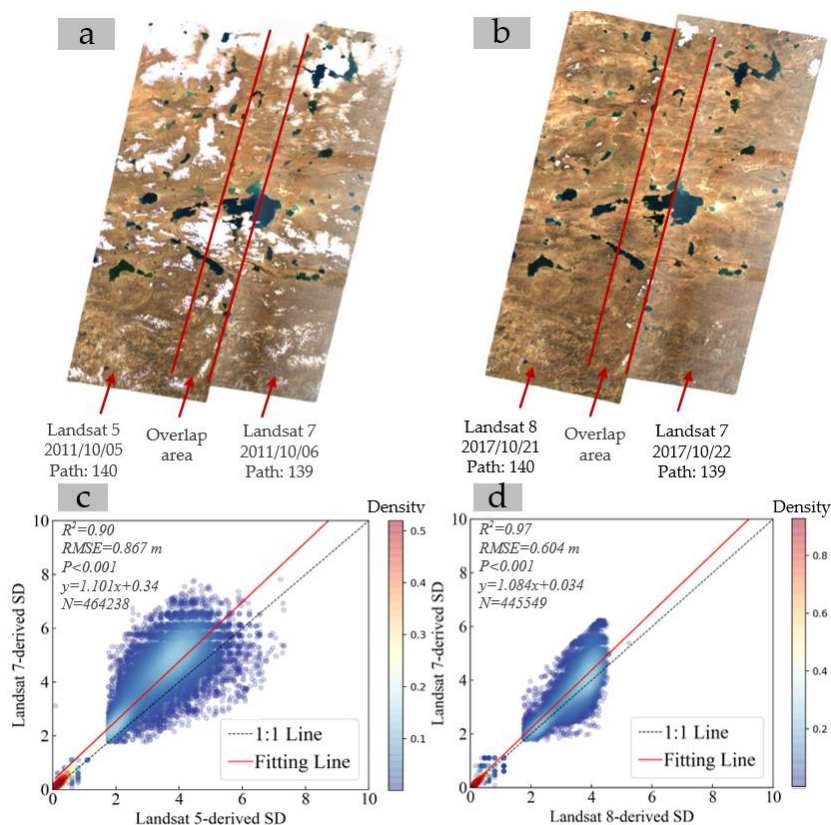
455 *5.1. Consistency between the Landsat estimation SD results*

456 Recently, many studies have proved the feasibility of using long-term Landsat series data
 457 from GEE to assess the changes in lake clarity (Zhang et al., 2021b; Yin et al., 2021). In order to
 458 evaluate the comparability of our LAWS30 dataset in monitoring long-term SD variations, the
 459 Landsat 5, 7, and 8 data for two adjacent tracks with overlapping areas were first selected to test
 460 the consistency between the Landsat estimation SD results (Fig. 12). The images of paths 139
 461 and 140 were chosen because the lakes in this place are hardly affected by human activities, and
 462 thus the SD of lakes can remain stable within a few days under stable hydrometeor conditions
 463 (Zhang et al., 2019b). The Landsat 5 images were taken on October 5, 2011, the Landsat 8 images
 464 were taken on October 21, 2017, and the Landsat 7 ETM+ images were taken on October 6, 2011
 465 and October 22, 2017. Since the compared images were quasi-synchronized with each other in
 466 one day, the SD of water bodies was assumed to be the same for both images. Fig. 12c,d show
 467 scatterplots of the SD results for the overlapping regions. It can be seen that, although the model
 468 coefficients of the three sensors were different in our calculation (Section 3.2), there was still
 469 strong consistency between the SD results of Landsat 5, 7, and 8, with an R^2 of 0.90 for Landsat
 470 5 vs. 7 and an R^2 of 0.97 for Landsat 8 vs. 7. The above results prove that the estimated SD results
 471 from Landsat 5, 7, and 8 data are highly consistent.

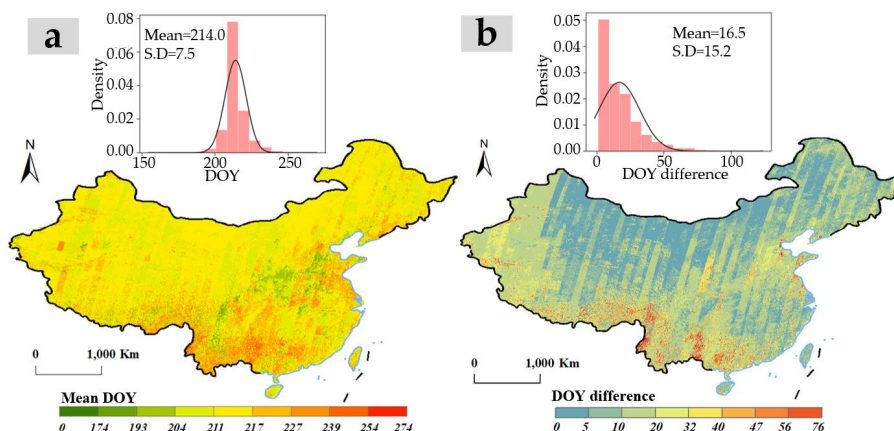
472 Moreover, since SD changes over time, and our LAWS30 dataset was calculated based on



473 the BAP composites, it was also necessary to test the phenological consistency between the time-
474 series summer BAP composites. The mean DOY of each pixel in the BAP composites from 1985
475 to 2020 was calculated and is shown in Fig. 13a. In addition, the maximum DOY difference of
476 each pixel location in the BAP composites from 1985 to 2020 was calculated and displayed in
477 Fig. 13b. From Fig. 13a, most areas of China were composites based on images around DOY 214,
478 and the mean standard deviation was only 7.5 days. Therefore, the developed BAP composites
479 can effectively ensure the consistency of phenology between different regions across China. In
480 addition, from Fig. 13b, the mean value of the maximum DOY difference across China was only
481 16.5 days, and the maximum DOY differences for most pixels across China (about 94%) were
482 within 32 days. Although the maximum DOY difference in parts of southern China exceeded 32
483 days due to the influence of clouds, most of these areas were mountainous with few lakes. In
484 addition, since the phenology of these regions were in summer, and the SD is relatively stable
485 during this season (Mccullough et al., 2012; Kloiber et al., 2002), the consistency of water clarity
486 in these areas can thus be considered not to have much impact on the final result. Therefore, the
487 results displayed in Figs. 12 and 13 confirm the reliability of our LAWS30 dataset for
488 evaluating the long-term SD across China.



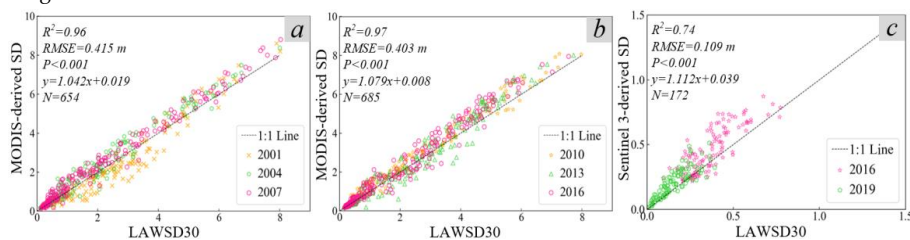
489
490 **Figure 12.** Overlapping regions of Landsat 5 and 7 data (a) and Landsat 8 and 7 data (b); lake SD
491 comparison for the Landsat 7 vs. Landsat 5 data (c) and the Landsat 7 vs. Landsat 8 data (d) for the lakes
492 from the overlap.



493
 494 **Figure 13.** The mean DOY of each pixel in the BAP composites from 1985 to 2020 (a) and the maximum
 495 DOY difference of each pixel location in the BAP composites from 1985 to 2020 (b). Note: S.D., standard
 496 deviation.

497 *5.2. Cross-comparison with existing water clarity monitoring studies*

498 To date, some past studies have also evaluated the water clarity of specific lakes in China
 499 (Shen et al., 2020; Wang et al., 2020). In order to further analyze the reliability of our estimated
 500 SD results across China, the results of this study were assessed against other existing water
 501 clarity monitoring studies. However, since most of the existing investigations focused on the
 502 annual average SD (Zhang et al., 2021b; Li et al., 2020a; Yin et al., 2021), and our LAWS30
 503 dataset is a summer SD dataset, it is a challenge to compare our results with other researches
 504 due to the different periods of interest. Fortunately, Wang et al. (2020) recently generated a time-
 505 series summer SD dataset (for the period 2000–2017) for lakes > 25 km² in China using water
 506 color parameters and MODIS data. Additionally, Shen et al. (2020) developed a multiyear
 507 monthly SD dataset (2016–2020) for 86 lakes in eastern China using Sentinel 3 images and a
 508 random forest regression SD model. Since both of the studies included SD results in summer,
 509 we had a unique opportunity to compare our SD estimates with them. The summer mean SD
 510 for each lake in the MODIS and the Sentinel 3-derived SD datasets was calculated and compared
 511 with our LAWS30 dataset. As shown in Fig. 14, our LAWS30 agreed well with both the
 512 MODIS and Sentinel 3-derived SD results. An average R^2 of 0.96 and an average RMSE of 0.409
 513 m was achieved when compared with the MODIS-derived results (Fig. 14a,b). In addition, an R^2
 514 of 0.74 and an RMSE of 0.109 m were shown in the comparison between the Sentinel 3-derived
 515 SD and our LAWS30 dataset (Fig. 14c). Thus, the above results confirm the reliability of our
 516 long-term LAWS30 dataset.



517



518 **Figure 14.** (a,b) Scatterplots of our LAWS30 data and the corresponding MODIS-derived SD data (Wang
519 et al., 2020) in the 2000s (2001, 2004, and 2007) and 2010s (in 2010, 2013, and 2016), respectively; (c)
520 scatterplot of our LAWS30 data and the corresponding Sentinel 3-derived SD data (Shen et al., 2020) in
521 2016 and 2019.

522 6. Conclusions

523 Water clarity is one of the most intuitive and important indicators to reflect the
524 comprehensive conditions in water bodies. In order to improve our understanding of the long-
525 term spatiotemporal patterns of lake water clarity in China, a long-term LAWS30 dataset with
526 a three-year temporal interval was first developed for the period 1985–2020 using Landsat series
527 data and the GEE platform. The dataset exhibited good performance when compared with
528 concurrent in situ SD measurements (with an R^2 of 0.86 and a RMSE of 0.225 m), thus confirming
529 the reliability of our LAWS30 dataset.

530 Subsequently, based on the generated LAWS30 dataset, the national-scale long-term SD
531 estimations of lakes in China ($N = 40,973$) over the past 35 years were analyzed. It was found
532 that the SD of lakes with an area ≤ 1 km² showed a significant decreasing trend during the period
533 1985–2020, but the decline rate began to slow down and stabilized after 2001. Regarding the SD
534 of the lakes with an area > 1 km², a significant downward trend was seen before 2001, and it
535 began to increase significantly afterwards. In addition, in terms of the spatial patterns, the small
536 lakes showing a decreasing SD trend during 1985–2020 accounted for the largest proportion in
537 MXR (about 30.0%), followed by YGR (23.8%), QTR (20.4%), NER (17.2%), and EPR (2.6%).
538 Additionally, for large lakes, this proportion was the largest in MXR (about 23.0%), followed by
539 QTR (19.4%), YGR (18.9%), EPR (17.7%), and NER (16.1%). The above results indicate that,
540 although the clarity of lakes in China has shown an improving trend since the 21st century, there
541 has still been a considerable proportion of lakes experiencing a downward SD trend over the
542 past few decades. This study can give an effective guidance for the management and restoration
543 of lake water environment.

544 **Author contributions:** Xidong Chen: Conceptualization, Methodology, Validation, Formal analysis,
545 Investigation, Writing - original draft. Liangyun Liu: Conceptualization, Investigation, Writing - review &
546 editing. Xiao Zhang: Methodology, Writing - review & editing. Junsheng Li: Resources, Writing - review
547 & editing. Shenglei Wang: Resources, Validation, Writing - review & editing. Yuan Gao: Validation, data
548 curation. Jun Mi: Validation, data curation.

549 **Data availability:** Our long-term LAWS30 dataset and the lake vector dataset generated for lakes with
550 an area > 0.01 km² are now available at <https://doi.org/10.5281/zenodo.5734071> and
551 <https://doi.org/10.5281/zenodo.5734166>, respectively. Additionally, our validation datasets can be
552 download at <http://lake.geodata.cn>.

553 **Competing interests.** The authors declare that they have no conflict of interest.

554 **Acknowledgments:** The authors gratefully acknowledge the data support from “National Earth System
555 Science Data Center, National Science & Technology Infrastructure of China (<http://www.geodata.cn>)”,
556 and the financial support provided for this research by the National Natural Science Foundation of China
557 (grant nos. 41825002, 41971318, 41901272) and the Strategic Priority Research Program of the Chinese
558 Academy of Sciences (grant no. XDA19090125).

559 References



- 560 Barnes, A.: Muddy Waters: The Public Health Risks and Sustainability of Bottled Water in China,
561 Vermont law review, 38, 971-1024, 2014.
- 562 Bastviken, D., Tranvik, L. J., Downing, J. A., Crill, P. M., and Enrich-Prast, A.: Freshwater
563 Methane Emissions Offset the Continental Carbon Sink, *Science*, 331, 50,
564 10.1126/science.1196808, 2011.
- 565 Biggs, J., von Fumetti, S., and Kelly-Quinn, M.: The importance of small waterbodies for
566 biodiversity and ecosystem services: implications for policy makers, *Hydrobiologia*, 793, 3-39,
567 10.1007/s10750-016-3007-0, 2017.
- 568 Brönmark, C. and Hansson, L.: Environmental issues in lakes and ponds: current state and
569 perspectives, *Environmental Conservation*, 29(3), 290-306, 10.1017/S0376892902000218, 2002.
- 570 Carlson, R. E.: TROPHIC STATE INDEX FOR LAKES, *Limnology and Oceanography*, 22, 361-
571 369, 10.4319/lo.1977.22.2.0361, 1977.
- 572 Chen, X., Liu, L., Zhang, X., Li, J., and Song, K.: An assessment of water color for inland water
573 in China using a Landsat 8-derived Forel-Ule index and the Google Earth Engine platform, *IEEE*
574 *Journal of Selected Topics in Applied Earth Observations and Remote Sensing*, PP(99), 1-1,
575 10.1109/JSTARS.2021.3085411, 2021.
- 576 CIE: Commission Internationale de l'Éclairage Proceedings, Cambridge University Press:
577 Cambridge, UK1932.
- 578 Cuffney, T. F., Meador, M. R., Porter, S. D., and Gurtz, M. E.: Responses of Physical, Chemical,
579 and Biological Indicators of Water Quality to a Gradient of Agricultural Land Use in the Yakima
580 River Basin, Washington, *Environmental Monitoring Assessment*, 64, 259-270,
581 10.1023/A:1006473106407, 2000.
- 582 Dai, Y., Feng, L., Hou, X., and Tang, J.: An automatic classification algorithm for submerged
583 aquatic vegetation in shallow lakes using Landsat imagery, *Remote Sensing of Environment*,
584 260, 10.1016/j.rse.2021.112459, 2021.
- 585 Dona, C., Sanchez, J. M., Caselles, V., Dominguez, J. A., and Camacho, A.: Empirical
586 Relationships for Monitoring Water Quality of Lakes and Reservoirs Through Multispectral
587 Images, *IEEE Journal of Selected Topics in Applied Earth Observations and Remote Sensing*, 7,
588 1632-1641, 10.1109/JSTARS.2014.2301295, 2014.
- 589 Downing, J. A., Cole, J. J., Duarte, C. M., Middelburg, J. J., Melack, J. M., Prairie, Y. T., Kortelainen,
590 P., Striegl, R. G., McDowell, W. H., and Tranvik, L. J.: Global abundance and size distribution of
591 streams and rivers, *Inland Waters*, 2, 229-236, 10.5268/iw-2.4.502, 2012.
- 592 Feng, L., Hou, X., and Zheng, Y.: Monitoring and understanding the water transparency changes
593 of fifty large lakes on the Yangtze Plain based on long-term MODIS observations, *Remote*
594 *Sensing of Environment*, 221, 675-686, 10.1016/j.rse.2018.12.007, 2019.
- 595 Garaba, S., Friedrichs, A., Voß, D., and Zielinski, O.: Classifying Natural Waters with the Forel-
596 Ule Colour Index System: Results, Applications, Correlations and Crowdsourcing, *International*
597 *Journal of Environmental Research Public Health*, 12, 16096-16109, 10.3390/ijerph121215044,
598 2015.
- 599 Garnesson, P., Mangin, A., D'Andon, O. F., Demaria, J., and Bretagnon, M.: The CMEMS
600 GlobColour chlorophyll a product based on satellite observation: multi-sensor merging and
601 flagging strategies, *Ocean Science*, 15, 819-830, 10.5194/os-15-819-2019, 2019.
- 602 Gomez, C., White, J. C., and Wulder, M. A.: Optical remotely sensed time series data for land
603 cover classification: A review, *ISPRS Journal of Photogrammetry and Remote Sensing*, 116, 55-



- 604 72, 10.1016/j.isprsjprs.2016.03.008, 2016.
- 605 Gorelick, N., Hancher, M., Dixon, M., Ilyushchenko, S., Thau, D., and Moore, R.: Google Earth
606 Engine: Planetary-scale geospatial analysis for everyone, *Remote Sensing of Environment*, 202,
607 18-27, 10.1016/j.rse.2017.06.031, 2017.
- 608 Griffiths, P., van der Linden, S., Kuemmerle, T., and Hostert, P.: Pixel-Based Landsat
609 Compositing Algorithm for Large Area Land Cover Mapping, *IEEE Journal of Selected Topics
610 in Applied Earth Observations and Remote Sensing*, 6, 2088-2101, 10.1109/jstars.2012.2228167,
611 2013.
- 612 Griffiths, P., Kuemmerle, T., Baumann, M., Radeloff, V. C., Abrudan, I. V., Lieskovsky, J.,
613 Munteanu, C., Ostapowicz, K., and Hostert, P.: Forest disturbances, forest recovery, and changes
614 in forest types across the Carpathian ecoregion from 1985 to 2010 based on Landsat image
615 composites, *Remote Sensing of Environment*, 151, 72-88, 10.1016/j.rse.2013.04.022, 2014.
- 616 Guo, L.: Ecology - Doing battle with the green monster of Taihu Lake, *Science*, 317, 1166-1166,
617 10.1126/science.317.5842.1166, 2007.
- 618 Hermosilla, T., Wulder, M. A., White, J. C., Coops, N. C., and Hobart, G. W.: An integrated
619 Landsat time series protocol for change detection and generation of annual gap-free surface
620 reflectance composites, *Remote Sensing of Environment*, 158, 220-234, 10.1016/j.rse.2014.11.005,
621 2015.
- 622 Hu, C.: A novel ocean color index to detect floating algae in the global oceans, *Remote Sensing
623 of Environment*, 113, 2118-2129, 10.1016/j.rse.2009.05.012, 2009.
- 624 Hu, H.: Population distribution, regionalization, and prospects in China, *Acta Geographica
625 Sinica*, 45, 139-145, 1990.
- 626 Islam, M. M.: Analyses of ASTER and Spectroradiometer Data with in Situ Measurements for
627 Turbidity and Transparency Study of Lake Abashiri, *International Journal of Geoinformatics*, 87,
628 76-77, 2006.
- 629 Kendall, M. G.: Rank Correlation Methods, *British Journal of Psychology*, 25, 86-91,
630 10.1111/j.2044-8295.1934.tb00727.x, 1990.
- 631 Kloiber, S. N., Brezonik, P. L., Olmanson, L. G., and Bauer, M. E.: A procedure for regional lake
632 water clarity assessment using Landsat multispectral data, *Remote Sensing of Environment*, 82,
633 38-47, 10.1016/s0034-4257(02)00022-6, 2002.
- 634 Lacaux, J. P., Tourre, Y. M., Vignolles, C., Ndione, J. A., and Lafaye, M.: Classification of ponds
635 from high-spatial resolution remote sensing: Application to Rift Valley Fever epidemics in
636 Senegal, *Remote Sensing of Environment*, 106, 66-74, 10.1016/j.rse.2006.07.012, 2007.
- 637 Lee, Z., Arnone, R., Boyce, D., Franz, B., and Wilson, C.: Global Water Clarity: Continuing a
638 Century-Long Monitoring, 10.1029/2018EO097251, 2018.
- 639 Li, J., Wang, S., Wu, Y., Zhang, B., Chen, X., Zhang, F., Shen, Q., Peng, D., and Tian, L.: MODIS
640 observations of water color of the largest 10 lakes in China between 2000 and 2012, *International
641 Journal of Digital Earth*, 9, 788-805, 10.1080/17538947.2016.1139637, 2016.
- 642 Li, N., Shi, K., Zhang, Y., Gong, Z., Peng, K., Zhang, Y., and Zha, Y.: Decline in Transparency of
643 Lake Hongze from Long-Term MODIS Observations: Possible Causes and Potential Significance,
644 *Remote Sensing*, 11, 10.3390/rs11020177, 2019.
- 645 Li, Y., Shi, K., Zhang, Y., Zhu, G., Zhang, Y., Wu, Z., Liu, M., Guo, Y., and Li, N.: Analysis of
646 water clarity decrease in Xin'anjiang Reservoir, China, from 30-Year Landsat TM, ETM plus ,
647 and OLI observations, *Journal of Hydrology*, 590, 10.1016/j.jhydrol.2020.125476, 2020a.



- 648 Li, Z., Cao, Y., Tang, J., Wang, Y., Duan, Y., Jiang, Z., and Qu, Y.: Relationships between Temporal
649 and Spatial Changes in Lakes and Climate Change in the Saline-Alkali Concentrated
650 Distribution Area in the Southwest of Songnen Plain, Northeast China, from 1985 to 2015, *Water*,
651 12(12), 3557, 10.3390/w12123557, 2020b.
- 652 Liangyun Liu, Xiao Zhang, Yuan Gao, Xidong Chen, Xie Shuai, and Mi, J.: Finer-Resolution
653 Mapping of Global Land Cover: Recent Developments, Consistency Analysis, and Prospects,
654 *Journal of Remote Sensing*, 2021, 38, 10.34133/2021/5289697, 2021.
- 655 Liu, C., Zhu, L., Li, J., Wang, J., Ju, J., Qiao, B., Ma, Q., and Wang, S.: The increasing water clarity
656 of Tibetan lakes over last 20 years according to MODIS data, *Remote Sensing of Environment*,
657 253, 10.1016/j.rse.2020.112199, 2021.
- 658 Liu, D., Duan, H., Loisel, S., Hu, C., Zhang, G., Li, J., Yang, H., Thompson, J. R., Cao, Z., Shen,
659 M., Ma, R., Zhang, M., and Han, W.: Observations of water transparency in China's lakes from
660 space, *International Journal of Applied Earth Observations and Geoinformation*, 92,
661 <https://doi.org/10.1016/j.rse.2020.111950> 2020.
- 662 Liu, X., Lee, Z., Zhang, Y., Lin, J., and Sun, Z.: Remote Sensing of Secchi Depth in Highly Turbid
663 Lake Waters and Its Application with MERIS Data, *Remote Sensing*, 11, 2226-
664 10.3390/rs11192226, 2019.
- 665 Liu, Y., Chen, C., and Li, Y.: Differentiation regularity of urban-rural equalized development at
666 prefecture-level city in China, *Journal of Geographical Sciences*, 25, 1075-1088, 10.1007/s11442-
667 015-1220-9, 2015.
- 668 Ma, H., Xu, J., and Wang, P.: Water Resource Utilization and China's Urbanization, *Resources*
669 *Science*, 36, 334-341, 1007-7588(2014)02-0334-08, 2014.
- 670 Ma, R., Yang, G., Duan, H., Jiang, J., Wang, S., Feng, X., Li, A., Kong, F., Xue, B., Wu, J., and Li,
671 S.: China's lakes at present: Number, area and spatial distribution, *Science China-Earth Sciences*,
672 54, 283-289, 10.1007/s11430-010-4052-6, 2011.
- 673 Mann, H. B.: Non-parametric tests against trend, *Econometrica*, 13(3), 245-259, 10.2307/1907187,
674 1945.
- 675 McCullough, I. M., Loftin, C. S., and Sader, S. A.: Combining lake and watershed characteristics
676 with Landsat TM data for remote estimation of regional lake clarity, *Remote Sensing of*
677 *Environment*, 123, 109-115, 10.1016/j.rse.2012.03.006, 2012.
- 678 Report on the State of the Ecology and Environment in China 2019:
679 <http://english.mee.gov.cn/Resources/Reports/>, last access: 30 December 2020.
- 680 Murshed, M. F., Aslam, Z., Lewis, R., Chow, C., Wang, D., Drikas, M., and Leeuwen, J. V.:
681 Changes in the quality of river water before, during and after a major flood event associated
682 with a La Nia cycle and treatment for drinking purposes, *Journal of Environmental Sciences*, 26,
683 1985-1993, 10.1016/j.jes.2014.08.001, 2014.
- 684 Novoa, S., Wernand, M. R., and van der Woerd, H. J.: The Forel-Ule scale revisited spectrally:
685 preparation protocol, transmission measurements and chromaticity, *Journal of the European*
686 *Optical Society-Rapid Publications*, 8, 10.2971/jeos.2013.13057, 2013.
- 687 Odermatt, D., Gitelson, A., Brando, V. E., and Schaepman, M.: Review of constituent retrieval in
688 optically deep and complex waters from satellite imagery, *Remote sensing of environment*, 118,
689 0-126, 10.1016/j.rse.2011.11.013, 2012.
- 690 Olmanson, L., Bauer, M., and Brezonik, P.: A 20-year Landsat water clarity census of Minnesota's
691 10,000 lakes, *Remote Sensing of Environment*, 112(11), 4086-4097, 10.1016/j.rse.2007.12.013, 2008.



- 692 Olmanson, L. G., Brezonik, P. L., Finlay, J. C., and Bauer, M. E.: Comparison of Landsat 8 and
693 Landsat 7 for regional measurements of CDOM and water clarity in lakes, *Remote Sensing of*
694 *Environment*, 185, 119–128, <https://doi.org/10.1016/j.rse.2016.01.007>, 2016.
- 695 Page, B. P., Olmanson, L. G., and Mishra, D. R.: A harmonized image processing workflow using
696 Sentinel-2/MSI and Landsat-8/OLI for mapping water clarity in optically variable lake systems,
697 *Remote Sensing of Environment*, 231, 111284, 10.1016/j.rse.2019.111284, 2019.
- 698 Palmer, S. C. J., Kutser, T., and Hunter, P. D.: Remote sensing of inland waters: Challenges,
699 progress and future directions, *Remote Sensing of Environment*, 157, 1–8,
700 10.1016/j.rse.2014.09.021, 2015.
- 701 Pekel, J. F., Cottam, A., Gorelick, N., and Belward, A. S.: High-resolution mapping of global
702 surface water and its long-term changes, *Nature*, 540, 418–422, 10.1038/nature20584, 2016.
- 703 Pitarch, J., van der Woerd, H. J., Brewin, R. J. W., and Zielinski, O.: Optical properties of Forel-
704 Ule water types deduced from 15 years of global satellite ocean color observations, *Remote*
705 *Sensing of Environment*, 231, 10.1016/j.rse.2019.111249, 2019.
- 706 Racetin, I., Krtalic, A., Srzic, V., and Zovko, M.: Characterization of short-term salinity
707 fluctuations in the Neretva River Delta situated in the southern Adriatic Croatia using Landsat-
708 5 TM, *Ecological Indicators*, 110, 10.1016/j.ecolind.2019.105924, 2020.
- 709 Shen, M., Duan, H., Cao, Z., Xue, K., Qi, T., Ma, J., Liu, D., Song, K., Huang, C., and Song, X.:
710 Sentinel-3 OLCI observations of water clarity in large lakes in eastern China: Implications for
711 SDG 6.3.2 evaluation, *Remote Sensing of Environment*, 247, 10.1016/j.rse.2020.111950, 2020.
- 712 Shi, K., Zhang, Y., Zhu, G., Qin, B., and Pan, D.: Deteriorating water clarity in shallow waters:
713 Evidence from long term MODIS and in-situ observations, *International Journal of Applied*
714 *Earth Observation and Geoinformation*, 68, 287–297, 10.1016/j.jag.2017.12.015, 2018.
- 715 Singh, S. P. and Singh, P.: Effect of temperature and light on the growth of algae species: A
716 review, *Renewable & Sustainable Energy Reviews*, 50, 431–444, 10.1016/j.rser.2015.05.024, 2015.
- 717 Song, K., Liu, G., Wang, Q., Wen, Z., Lyu, L., Du, Y., Sha, L., and Fang, C.: Quantification of lake
718 clarity in China using Landsat OLI imagery data, *Remote Sensing of Environment*, 243,
719 10.1016/j.rse.2020.111800, 2020.
- 720 Song, K., Wen, Z., Xu, Y., Yang, H., Lyu, L., Zhao, Y., Fang, C., Shang, Y., and Du, J.: Dissolved
721 carbon in a large variety of lakes across five limnetic regions in China, *Journal of Hydrology*,
722 563, 143–154, 10.1016/j.jhydrol.2018.05.072, 2018.
- 723 Steyerberg, E. W.: Regression Modeling Strategies: With Applications, to Linear Models, Logistic
724 and Ordinal Regression, and Survival Analysis, *Biometrics*, 72, 1006–1007, 10.1007/978-3-319-
725 19425-7, 2016.
- 726 Preliminary Assessment of the Value of Landsat 7 ETM+ Data Following Scan Line Corrector
727 Malfunction: Available online at:
728 http://Landsat.usgs.gov/data_products/slc_off_data_products/documents/SLC_off_Scientific_Usability.pdf. Accessed 12 April 2006, last
729
- 730 van der Woerd, H. J. and Wernand, M. R.: True Colour Classification of Natural Waters with
731 Medium-Spectral Resolution Satellites: SeaWiFS, MODIS, MERIS and OLCI, *Sensors*, 15, 25663–
732 25680, 10.3390/s151025663, 2015.
- 733 van der Woerd, H. J. and Wernand, M. R.: Hue-Angle Product for Low to Medium Spatial
734 Resolution Optical Satellite Sensors, *Remote Sensing*, 10, 10.3390/rs10020180, 2018.
- 735 Wang, S.: Large-scale and Long-time Water Quality Remote Sensing Monitoring over Lakes



- 736 Based on Water Color Index, University of Chinese Academy of Sciences, Beijing, 2018.
- 737 Wang, S., Li, J., Zhang, W., Cao, C., and Zhang, B.: A dataset of remote-sensed Forel-Ule Index
738 for global inland waters during 2000–2018, *Scientific Data*, 8, 10.1038/s41597-021-00807-z, 2021.
- 739 Wang, S., Li, J., Zhang, B., Spyarakos, E., Tyler, A. N., Shen, Q., Zhang, F., Kutser, T., Lehmann,
740 M. K., Wu, Y., and Peng, D.: Trophic state assessment of global inland waters using a MODIS-
741 derived Forel-Ule index, *Remote Sensing of Environment*, 217, 444–460, 10.1016/j.rse.2018.08.026,
742 2018.
- 743 Wang, S., Li, J., Zhang, B., Lee, Z., Spyarakos, E., Feng, L., Liu, C., Zhao, H., Wu, Y., Zhu, L., Jia,
744 L., Wan, W., Zhang, F., Shen, Q., Tyler, A. N., and Zhang, X.: Changes of water clarity in large
745 lakes and reservoirs across China observed from long-term MODIS, *Remote Sensing of
746 Environment*, 247, 10.1016/j.rse.2020.111949, 2020.
- 747 Wang, X. and Yang, W.: Water quality monitoring and evaluation using remote-sensing
748 techniques in China: A systematic review, *Ecosystem Health and Sustainability*, 5, 47–56,
749 10.1080/20964129.2019.1571443, 2019.
- 750 White, J. C., Wulder, M. A., Hobart, G. W., Luther, J. E., Hermosilla, T., Griffiths, P., Coops, N.
751 C., Hall, R. J., Hostert, P., Dyk, A., and Guindon, L.: Pixel-Based Image Compositing for Large-
752 Area Dense Time Series Applications and Science, *Canadian Journal of Remote Sensing*, 40, 192-
753 212, 10.1080/07038992.2014.945827, 2014.
- 754 Xie, S., Liu, L., Zhang, X., Yang, J., Chen, X., and Gao, Y.: Automatic Land-Cover Mapping using
755 Landsat Time-Series Data based on Google Earth Engine, *Remote Sensing*, 11,
756 10.3390/rs11243023, 2019.
- 757 Xue, K., Ma, R., Duan, H., Shen, M., Boss, E., and Cao, Z.: Inversion of inherent optical properties
758 in optically complex waters using sentinel-3A/OLCI images: A case study using China's three
759 largest freshwater lakes, *Remote Sensing of Environment*, 225, 328–346, 10.1016/j.rse.2019.03.006,
760 2019.
- 761 Yin, Z., Li, J., Liu, Y., Xie, Y., and Zhang, B.: Water clarity changes in Lake Taihu over 36 years
762 based on Landsat TM and OLI observations, *International Journal of Applied Earth Observation
763 Geoinformation*, 102, 102457, 10.1016/j.jag.2021.102457, 2021.
- 764 Yuan, Z., Liang, C., and Li, D.: Urban stormwater management based on an analysis of climate
765 change: A case study of the Hebei and Guangdong provinces, *Landscape and Urban Planning*,
766 177, 217–226, 10.1016/j.landurbplan.2018.04.003, 2018.
- 767 Zhang, G., Yao, T., Chen, W., Zheng, G., Shum, C. K., Yang, K., Piao, S., Sheng, Y., Yi, S., Li, J.,
768 O'Reilly, C. M., Qi, S., Shen, S. S. P., Zhang, H., and Jia, Y.: Regional differences of lake evolution
769 across China during 1960s–2015 and its natural and anthropogenic causes, *Remote Sensing of
770 Environment*, 221, 386–404, 10.1016/j.rse.2018.11.038, 2019a.
- 771 Zhang, G. Q., Yao, T. D., Chen, W. F., Zheng, G. X., Shum, C., Yang, K., Piao, S. L., Sheng, Y. W.,
772 Yi, S., and Li, J. L.: Regional differences of lake evolution across China during 1960s–2015 and
773 its natural and anthropogenic causes, *Remote Sensing of Environment*, 221, 386–404,
774 <https://doi.org/10.1016/j.rse.2018.11.038>, 2019b.
- 775 Zhang, X., Liu, L., Chen, X., Gao, Y., and Jiang, M.: Automatically Monitoring Impervious
776 Surfaces Using Spectral Generalization and Time Series Landsat Imagery from 1985 to 2020 in
777 the Yangtze River Delta, *Journal of Remote Sensing*, 2021, 9873816, 10.34133/2021/9873816, 2021a.
- 778 Zhang, X., Liu, L., Wu, C., Chen, X., Gao, Y., Xie, S., and Zhang, B.: Development of a global 30m
779 impervious surface map using multisource and multitemporal remote sensing datasets with the



780 Google Earth Engine platform, Earth System Science Data, 12, 1625-1648, 10.5194/essd-12-1625-
781 2020, 2020.
782 Zhang, Y., Zhang, Y., Shi, K., Zhou, Y., and Li, N.: Remote sensing estimation of water clarity for
783 various lakes in China, Water Research, 192, 116844, <https://doi.org/10.1016/j.watres.2021.116844>,
784 2021b.
785 Zhigang, C., Hongtao, D., Lian, F., Ronghua, M., and Kun, X.: Climate- and human-induced
786 changes in suspended particulate matter over Lake Hongze on short and long timescales,
787 Remote Sensing of Environment, <https://doi.org/10.1016/j.rse.2017.02.007>, 2017.
788 Zhou, Q. C., Wang, W. L., Huang, L. C., Zhang, Y. L., Qin, J., Li, K. D., and Chen, L.: Spatial and
789 temporal variability in water transparency in Yunnan Plateau lakes, China, Aquatic Sciences, 81,
790 10.1007/s00027-019-0632-5, 2019.
791